Full-Sphere Characterization of Low-Gain Antennas via Truncated Field Pattern Stitching

Jure Soklič[1] and Holger Arthaber[2]
Institute of Electrodynamics, Microwave and Circuit Engineering
Technische Universität Wien
Vienna, Austria
(jure.soklic[1], holger.arthaber[2])@tuwien.ac.at

***Abstract*—Our work proposes a novel method for obtaining full-sphere radiation patterns from truncated measurements. This is achieved by stitching partially overlapping truncated field patterns, which together cover the whole measurement sphere. Measuring an antenna in different orientations results in a misalignment between measurements which is not perfectly known and needs to be accounted for in order to stitch the patterns together. The method first makes use of an iterative procedure to compute spherical wave coefficients (SWCs) capable of accurately describing the truncated patterns. A bounded minimization of the NMSE in the overlapping range between patterns is then done, varying through a range of translations and rotations for one pattern while keeping the other pattern fixed. After alignment, the patterns can be stitched together. The method was validated on both SWC-based and EM simulation models for randomly chosen misalignments. For all models, the NMSE after pattern stitching was found to be below -52 dB. In the final validation step, the method was tested on actual measurement results of two low-gain antennas. For each of the validation steps, potential sources of error are identified. The method demonstrates promising results in achieving full-sphere characterization of low-gain antennas in typical non-full-sphere measurement chambers.**

I. Introduction

Physical constraints of spherical antenna measurement systems often impose a limit on the maximum spherical angle that can be covered in a single measurement. Thus, we are required to deal with less-than-full-sphere antenna radiation patterns, called truncated patterns. In spherical near-field measurement systems, patterns are measured in antenna's near-field and transformed to far-field via a spherical near-to-far-field transformation (SN2FFT) algorithm. Fourier-transform(FT)-based algorithms, as described in [1] [2], are typically used for this task. They require equidistant sampling over the whole sphere, so missing points have to be assigned a value, typically zero. For low-gain antennas (LGAs), where radiation is not negligible in most directions, the impact of truncation is severe, causing both non-zero higher order spherical wave coefficients (SWCs) and errors in the transformed field patterns in the covered range.

An approach to reduce truncation errors was suggested in [3], where the authors propose an iterative procedure for the SN2FFT algorithm. The values in the truncated region are set to zero, and the algorithm is used to obtain a solution in terms of SWCs. After filtering out SWCs above maximum polar order $N_{\max}$, the field is reconstructed and the newly computed field values are used in the truncated region, while the values in the measured region are replaced with the actual measured values. This is done iteratively until the reconstructed fields match the measured fields up to a defined error limit. This approach is further simplified in [4] by strictly limiting SWCs to $N_{\max}$, thus avoiding the need for SWC-filtering. This method computes a possible combination of SWCs capable of describing the pattern in the measured range, but the solution does not provide reliable information on the behavior in the range above truncation angle θ_{trunc}.

While truncation errors for high-gain antennas can often be kept low by orienting them in a way that radiated fields in the truncated region are negligible, this approach is not possible when dealing with LGAs. In order to determine antenna efficiency, gain, or other common antenna parameters, full-sphere radiation patterns of LGAs are required. It was recently shown that coordinate system manipulation of iteratively obtained SWCs is possible for a large range of translation distances and rotation angles [5]. These findings demonstrate the possibility of aligning multiple truncated patterns of an antenna, measured in different orientations, to the same coordinate system and stitching them together to obtain full-sphere radiation patterns. To do so, a new method is proposed, which will be presented in the following sections.

II. The Proposed Method for Full-Sphere Characterization of Low-Gain Antennas

The fundamental idea behind the proposed method is that an antenna can be measured in multiple orientations, such that measurement points over the whole sphere are obtained. To demonstrate the working principle, two measured orientations will be considered in this work, however, there is no indication that a generalization of the approach would not be possible with more than two measurement orientations. With two measurements, the intuitive approach is to rotate the antenna by 180° in one measurement, thus obtaining measurements of two hemispheres. It has to be taken into account that, in practice, the measured antenna is unlikely to be placed exactly in the origin of the measurement system. Moreover, changing the orientation of the antenna will likely result in some misalignment between the measurements. Thus, the coordinate systems of the measured patterns have to be aligned, for which

an overlapping region is needed. The proposed method can conceptually be divided into three parts:

1) SWCs capable of accurately describing the patterns in their respective truncated regions are obtained by the iterative reconstruction procedure.
2) Relative misalignment between the truncated patterns is found by a normalized mean squared error (NMSE) minimization procedure.
3) One pattern is manipulated by means of rotation and translation to align it with the other and the two are stitched together into full-sphere radiation patterns of the antenna.

In Figure 1, the concept of pattern stitching procedure is illustrated. Two antenna measurements are done, where the antenna has been rotated by 180° around the x- or y-axis for measurement 2. The measurement points of both measurements are shown along with the truncation region marked in green (top). When measurement 2 is rotated by 180°, the points of the two measurements are most likely misaligned and need to be aligned (upper middle). After the coordinate systems have been successfully aligned, the measurement points of the two measurements coincide (lower middle) and can be stitched together to obtain full-sphere patterns (bottom).

A. Iterative Algorithm for Computing SWCs

When transforming spherical near-field antenna patterns to far-field, the first thing one needs to do is to compute the SWCs. These are complex weighting factors for solutions of the wave equation in a spherical coordinate system, called spherical wave functions. A superposition of these wave functions, weighted by their corresponding SWCs, can describe the radiation in any point in space. As stated earlier, truncation causes errors in radiation patterns, especially in the case of LGAs. These errors are dealt with by following the idea in [4], which gives a combination of SWCs capable of describing the antenna in the measured points. The fields in the truncated region are set to the last measured point instead of zero, which was found to allow for faster convergence of the algorithm. The goal is to minimize the NMSE between the measured points and the points obtained from field patterns of computed SWCs.

B. Translation and Rotation Vector Optimization

For any pair of coordinate systems, one can be described by the other with a combination of translation and rotation. Mathematical operators capable of perfectly describing SWCs in one coordinate system as a combination of SWCs in another have been invented in the 1960s and 1970s and the operators required by the proposed method are summarized in [1]. These operators form the basis for the optimization procedure. It should be noted again that SWCs obtained from truncated fields by the iterative algorithm represent a possible solution, capable of describing the radiation patterns at measured points and at the same distance as measured. However, a change in measurement distance or observation points results in errors in the radiation patterns. An investigation of performance of these operators on such truncated SWCs has shown that,

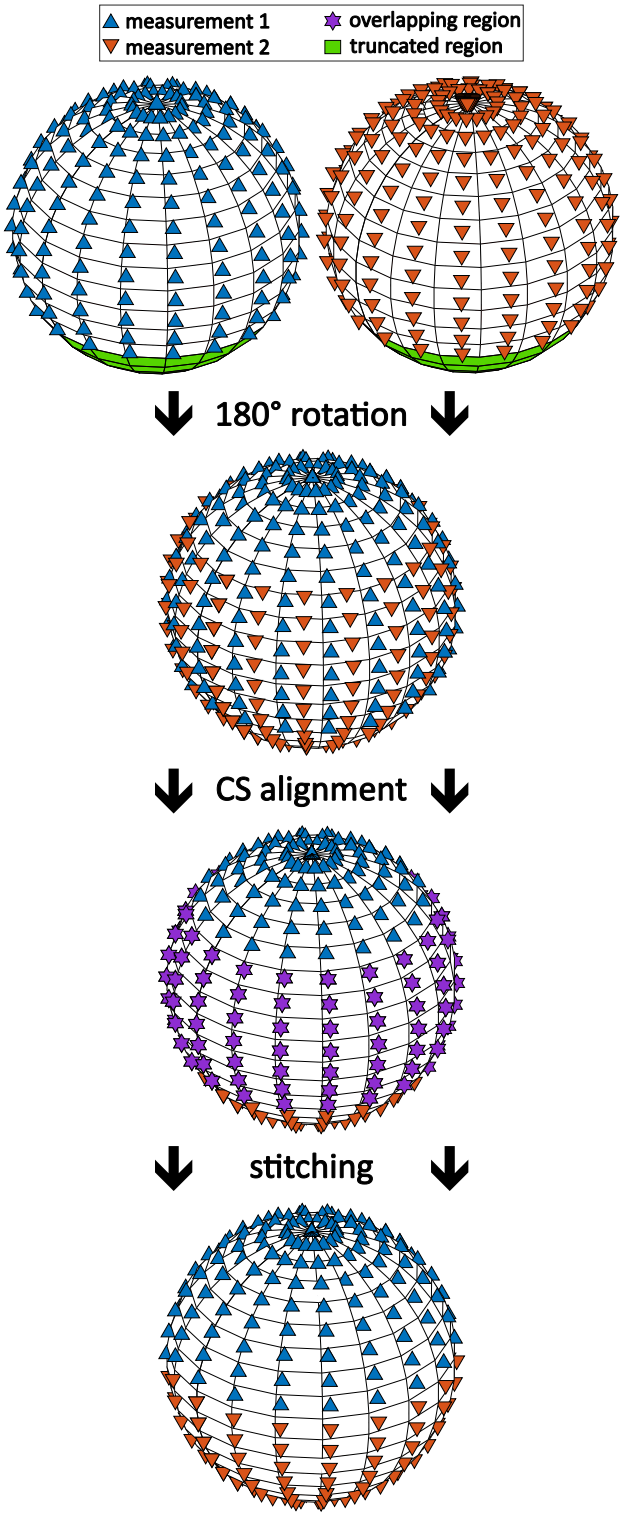

Fig. 1. Pattern stitching procedure: Antenna measurement points in two orientations (top), after rotation of measurement 2 by 180° about x- or y-axis (upper middle), pattern measurement points after coordinate system alignment (lower middle), and stitched patterns (bottom).

while translation and rotation introduces additional errors, they are contained in the region near θ_{trunc} [5]. SWCs of one measurement are first rotated by 180° as shown in Figure 1 (upper middle). Under the requirement that an overlap between the two measurements exists, the NMSE in the overlapping field is evaluated. Due to the fact that the error in reconstructed translated and rotated truncated fields is largest near truncation [5], a weighting factor is used for the evaluation of NMSE. Since the two truncated patterns have largest errors on opposite sides of the overlapping region and the most accurate data is expected near $\theta = 90^\circ$, data at 90° has to be weighted with the highest factor and decrease equally when moving away from it in either direction. The family of functions $f(\theta, x) = \sin^x(\theta)$ was found convenient for the desired weighting, where the power x determines how fast the weights decrease when moving away from $\theta = 90^\circ$. The function $\sin^2(\theta)$ was found to give good results for the proposed method and is used as the weighting factor, but further investigation of different weighting factors could be beneficial. Finally, to find the misalignment between two measurements, minimization of weighted NMSE is carried out, where one truncated pattern is fixed and the other is rotated and translated in a constrained range of translations (x, y, z) and rotations $(\vartheta, \varphi, \chi)$.

C. Stitching of Partial Patterns

Once the minimization procedure converges, the found optimal translation $(x_{\mathrm{opt}}, y_{\mathrm{opt}}, z_{\mathrm{opt}})$ and rotation $(\vartheta_{\mathrm{opt}}, \varphi_{\mathrm{opt}}, \chi_{\mathrm{opt}})$ vectors are used on the SWCs representing the measurement which was rotated and translated during minimization. Radiation patterns of these aligned SWCs are then computed and the results (for $\theta > 90^\circ$) are stitched with the unchanged patterns (for $\theta < 90^\circ$) of the other measurement, while the middle point between them ($\theta = 90^\circ$, if measured) is obtained as a mean value of the two measurements. In the final processing step, SN2FFT is used on the stitched patterns to obtain accurate SWCs and the full-sphere far-field radiation pattern of the antenna.

III. Test Objects used for Validation of the Proposed Method

To determine how accurately the proposed method can characterize low-gain antennas over the full sphere, the method was tested on various test objects. In order to gain better insight into potential sources of errors, two types of test objects were used: SWC-based models and EM-simulation models. All test objects were modelled for operation at 2.4 GHz for comparability purposes and the radiation patterns of all models were obtained at a distance of 1.31 m, corresponding to the measurement distance between the probe antenna and antenna under test (AUT) in the anechoic chamber at TU Wien. In accordance with the limits of the measurement setup for measuring LGAs in the anechoic chamber (using additional absorbers in phi stage), all patterns were truncated at $\theta = 140^\circ$. In all cases, the pattern representing the upper hemisphere pattern (measurement 1 in Figure 1) was kept fixed while the lower hemisphere pattern (measurement 2 in Figure 1) was misaligned by two different randomly chosen translation and rotation combinations, listed in Table I.

TABLE I
Test Misalignment Combinations

	rotation $(\vartheta, \varphi, \chi)$	**translation** $(\mathbf{x}, \mathbf{y}, \mathbf{z})$
misalignment 1	$(10, -2, 0)^\circ$	$(2, -2, 4)$ cm
misalignment 2	$(10, 5, 10)^\circ$	$(10, 10, 10)$ cm

A. SWC-Based Models

A simple x-oriented dipole and sets of randomly generated SWCs of order $N_{\max} \in \{4, 19, 34\}$ were used to construct antenna field patterns. Two patterns were created for each test object, where one was simply truncated at 140° and the other rotated by 180° over y-axis to represent the measurement of the other antenna orientation and then truncated in the same manner as the first one. For both models, the 180°-rotated pattern was translated and rotated, once by the combination from **misalignment 1** and once by the combination from **misalignment 2**, which were listed earlier in Table I.

B. EM-Simulation Models

Next, two low-gain antennas were simulated in HFSS [6], a bowtie antenna and a planar inverted-F antenna (PIFA). Near-fields for all selected orientations (original orientation for upper hemisphere and both misaligned orientations from Table I for the lower hemisphere) were exported from the simulation software. The 3D models along with their corresponding original orientation coordinate systems are shown in Figures 2 and 3.

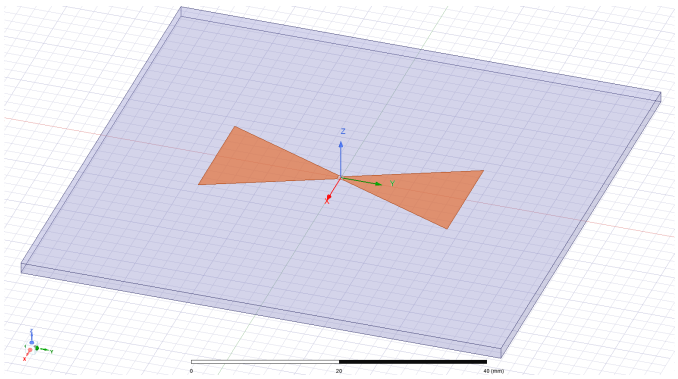

Fig. 2. HFSS: bowtie 3D model.

IV. Results of Method Validation

The test objects presented in the previous section were processed with our proposed method and a comparison was made between the original full-sphere patterns and stitched truncated patterns obtained by the method in terms of the computed NMSE. Results are shown in Table II and it can be observed that the NMSE for the smaller **misalignment 1** is, in average, about 7.5 dB lower than for **misalignment 2**. This confirms that, as expected from findings in [5], the

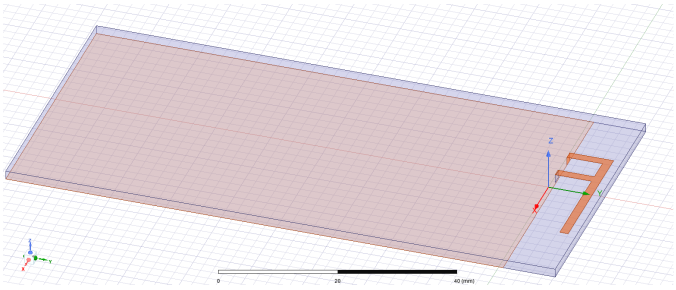

Fig. 3. HFSS: PIFA 3D model.

NMSE of the reconstructed pattern increases with increasing misalignment. However, even with the large misalignment, considered to represent the placement precision achievable with the naked eye, the NMSE for all test objects was below -52 dB. Additionally, results in Table II indicate that no significant differences in accuracy exist between SWC-based and EM-simulation models. While a simple same-distance near-to-near-field transform of EM-simulation models shows an NMSE increase in comparison to SWC-based models, the error introduced by the iterative truncated field reconstruction and coordinate system manipulation of our proposed method was found to be the dominating source of the overall NMSE.

TABLE II
NMSE — SWC-BASED MODELS AND EM-SIMULATION MODELS.

	NMSE (dB)	
SWC-based models	**misalignment 1**	**misalignment 2**
x-oriented dipole	-62.09	-53.80
random SWCs ($N = 4$)	-64.67	-53.16
random SWCs ($N = 19$)	-64.71	-61.34
random SWCs ($N = 34$)	-62.39	-58.50
EM-simulation models	**misalignment 1**	**misalignment 2**
bowtie	-65.14	-52.91
PIFA	-63.54	-56.07

To gain insight into error distribution, normalized error was investigated on the whole sphere. Error changes in θ-direction were most distinct and plots with overlaid ϕ-cuts were created. As an example of SWC-based models, the results for the random SWC pattern with $N_{\max} = 19$ are shown in Figures 4 and 5 for **misalignment 1** and **2**, respectively. One can see that the error has local maxima near the junctions between stitched patterns ($\theta \in \{0°, 90°, 180°\}$). This does not come unexpected, since any misalignment or general difference between the two patterns results in a slight discontinuity which results in an increased error. Moreover, an overall 5–10 dB error increase can be observed in the lower hemisphere ($\theta > 90°$) when compared to the upper hemisphere ($\theta < 90°$). Since the upper hemisphere measurement is fixed during processing, while the lower hemisphere measurement is rotated and translated to compensate for the misalignment, this error increase can be assigned to the rotation and translation of truncated pattern fields. The normalized error plots for the PIFA EM-simulation example are shown in Figures 6 and 7.

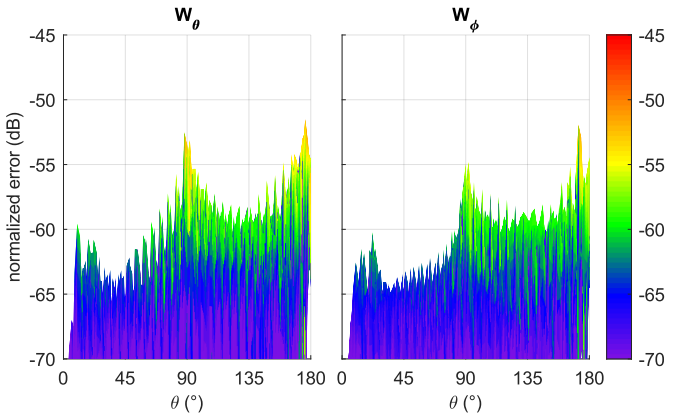

Fig. 4. Random SWCs ($N_{\max} = 19$): Normalized error over θ (overlaid ϕ-cuts) for **misalignment 1**.

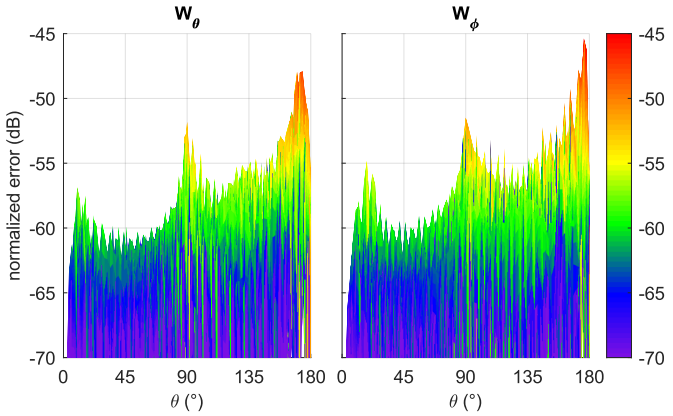

Fig. 5. Random SWCs ($N_{\max} = 19$): Normalized error over θ (overlaid ϕ-cuts) for **misalignment 2**.

They show similar results to those of the SWC-based models example.

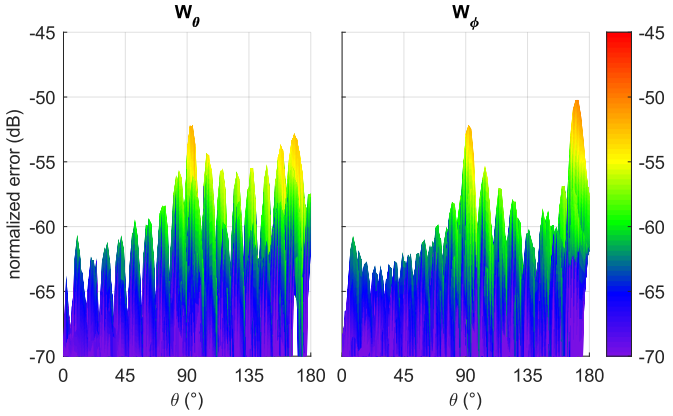

Fig. 6. PIFA: Normalized error over θ (overlaid ϕ-cuts) for **misalignment 1**.

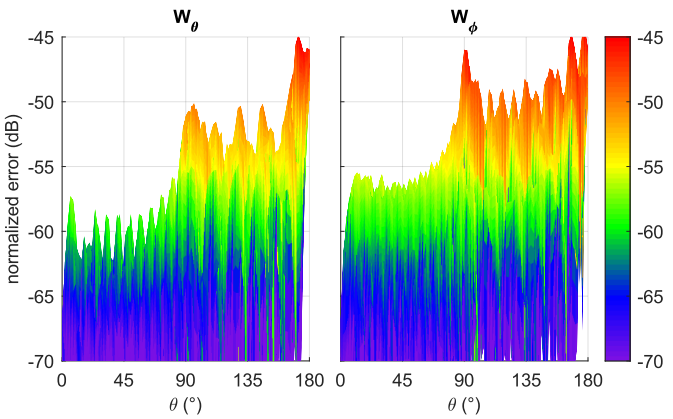

Fig. 7. PIFA: Normalized error over θ (overlaid ϕ-cuts) for **misalignment 2**.

V. Measurement Results

Having established that both SWC-based and EM-simulation full-sphere radiation patterns can accurately be reconstructed by stitching truncated radiation patterns, the final step was to test the performance of the method on actual antenna measurements. Field patterns were measured in the anechoic chamber at TU Wien, which can cover θ angles up to $140°$ when using additional absorbers for LGAs. Two antennas were measured, a simple folded dipole antenna operating in the range between 1.8 GHz and 2 GHz and a UWB conical monopole antenna, presented in [7], manufactured in-house with a simplified ground plane. The UWB antenna was measured in the range between 4 and 16 GHz. Both antennas are shown in one of the measured orientations in Figures 8 and 9.

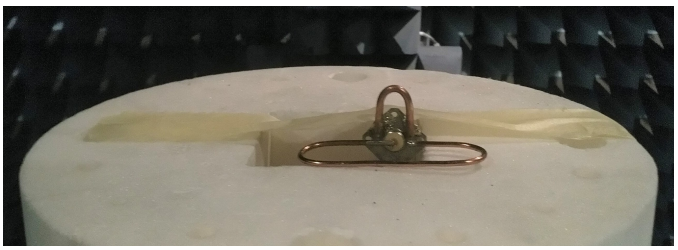

Fig. 8. Folded dipole antenna.

A. Radiation Patterns

The measurements were then processed for all measured frequencies. It should be noted that processing times strongly depend on the maximum polar order, $N_{\max}$, and processing higher frequencies of the UWB antenna took up to three hours. Due to the supporting structure, the UWB antenna was significantly offset from the origin of the measurement coordinate system (see Figure 9). Therefore, measurements of both orientations were first translated by 8 cm in $-z$ direction to reduce the maximum radial extent (MRE) of the antenna and, with it, the maximum polar order $N_{\max}$ required for processing the patterns. Exemplary far-field patterns of

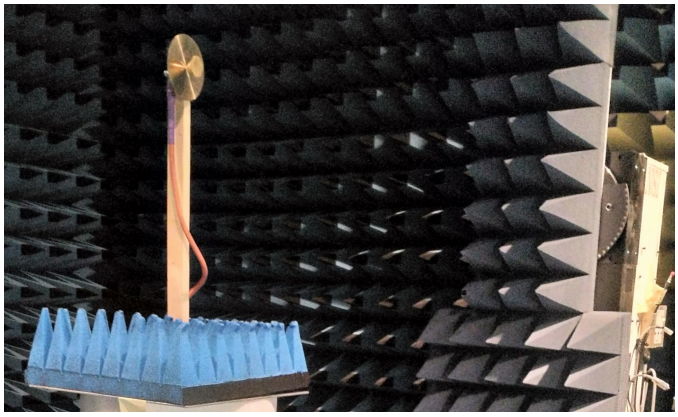

Fig. 9. UWB conical monopole antenna.

both antennas obtained by the proposed method are shown in Figures 10 and 11 for the center frequency of the measured range. It can be seen that the method delivers smooth results and no discontinuity in the transition between the top and bottom hemisphere measurements can be observed.

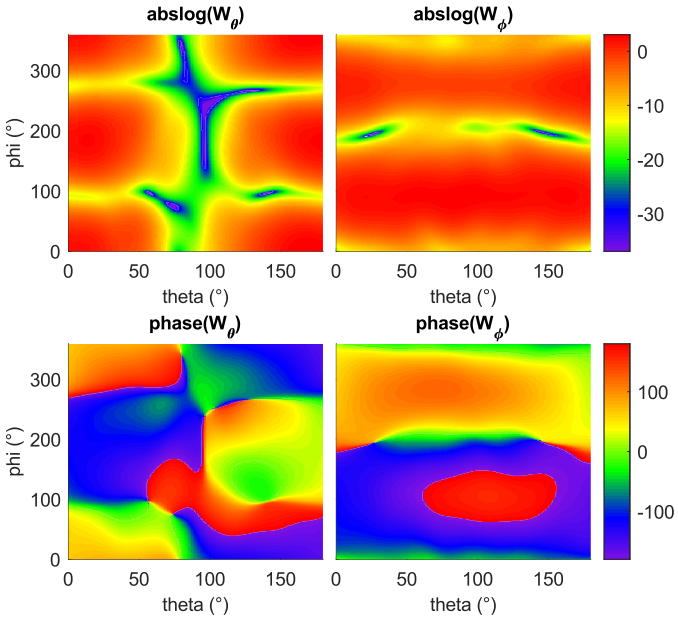

Fig. 10. Far-field radiation patterns of the folded dipole at 1.9 GHz: Magnitude (top) and phase (bottom).

An evaluation of NMSE as in the previous step was not possible since full-sphere measurements required for reference are not possible at TU Wien. Weighted NMSE values for the overlapping region were evaluated instead and are listed in Table III. As can be seen, the weighted NMSE values in the overlapping region are much larger than the NMSE values observed in the validation process, but they remain near or below -20 dB, meaning the error in the overlapping region is still less than 1%.

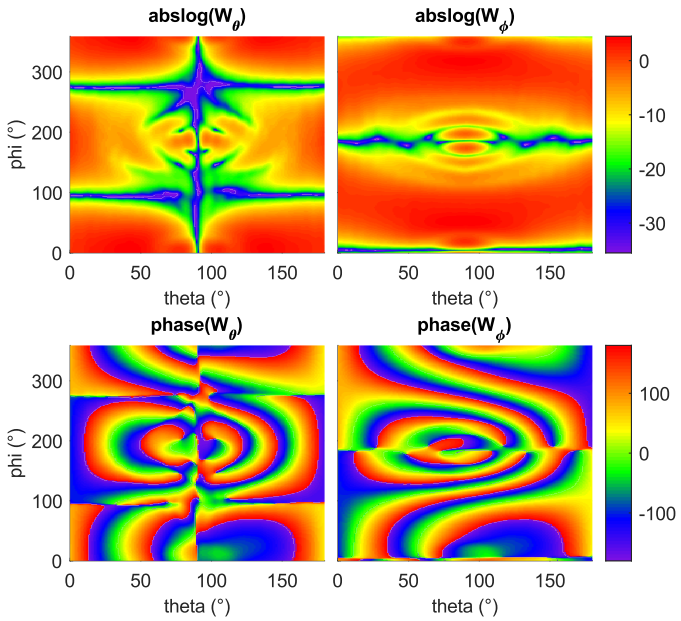

Fig. 11. Far-field radiation patterns of the UWB conical monopole antenna at 10 GHz: Magnitude (top) and phase (bottom).

TABLE III
WEIGHTED NMSE IN THE OVERLAPPING REGION - MEASURED ANTENNAS.

	weighted NMSE (dB)	
measured antenna	**mean**	**max**
folded dipole	−21.09	−19.93
UWB antenna	−24.37	−21.59

B. Sources of Error

The observed increase in error for practical measurements was investigated and lead to the following findings. Both SWC-based models and EM-simulation models assumed the antenna to stand in a perfect free-space environment without any interfering objects. In practice, however, such a setup is impossible. Along with typical sources of error in anechoic measurement chambers, such as reflections, noise, probe position error, etc., two additional sources of error specific to the pattern stitching case were found:

1) Antenna's mounting support orientation changes between measurements in different orientation.
2) Cable orientation changes between measurements in different orientation.

As much as possible, care has to be taken to minimize the effects of these two sources of error, i.e., by placing the mounting support and the cable in an area where antenna radiation is low and away from the overlapping region of both measurements. Furthermore, materials used for support structures should be carefully chosen and used whenever possible, i.e., materials which electrically approach the dielectric properties of air, such as ROHACELL® HF.

VI. CONCLUSION

The validation of our proposed method on SWC-based models and EM-simulation models was shown to reconstruct full-sphere patterns from truncated fields with high accuracy that can be considered sufficient for most practical applications. Tests on actual measurements have shown a significant error increase, which was attributed to the different orientation of the coaxial cable attached to the antenna and antenna's mounting support. The weighted NMSE in the overlapping range was still found to be below 1%, showing that the proposed method can be used for full-sphere pattern characterization from truncated field pattern measurements. Future work will attempt to tackle the sources of error in practical measurements and further increase the accuracy of the method.

REFERENCES

[1] J. E. Hansen, Ed., *Spherical Near-field Antenna Measurements*, ser. IET Electromagnetic Waves Series. The Institution of Engineering and Technology, 1988, vol. 26.
[2] "IEEE recommended practice for near-field antenna measurements," *IEEE Std 1720-2012*, pp. 1–102, 2012.
[3] E. Martini, S. Maci, and L. J. Foged, "Spherical near field measurements with truncated scan area," in *Proceedings of the 5th European Conference on Antennas and Propagation (EUCAP)*, 2011, pp. 3256–3258.
[4] R. Cornelius, H. Shakhtour, and D. Heberling, "Extrapolation of truncated spherical near-field measurements," in *2012 42nd European Microwave Conference*, 2012, pp. 301–304.
[5] J. Soklič and H. Arthaber, "Investigation of coordinate system rotation and translation on iteratively reconstructed truncated antenna field patterns," in *2022 IEEE International Symposium on Antennas and Propagation and USNC-URSI Radio Science Meeting (AP-S/URSI)*, 2022, pp. 631–632.
[6] Ansys, "HFSS 2022 R1," Accessed: July 4, 2022. [Online]. Available: https://www.ansys.com/products/electronics/ansys-hfss
[7] T. Mikulasek, J. Blumenstein, and A. Prokes, "Antennas utilized for intra-vehicle 3–11GHz and 55–65GHz channel measurement," in *2016 Progress in Electromagnetic Research Symposium (PIERS)*, 2016, pp. 4258–4262.